Electronic Supplementary Material (ESI) for Lab on a Chip

Supplementary Information

A Microfluidic Approach to Synthesizing High-Performance Microfibers with Tunable Anhydrous Proton Conductivity

Mohammad Mahdi Hasani-Sadrabadi[†,§], Jules J. VanDersarl[†,*], Erfan Dashtimoghadam[‖], Ghassem Bahlakeh[⊥], Fatemeh Sadat Majedi[†], Nassir Mokarram[§], Arnaud Bertsch[†], Karl I. Jacob[§], Philippe Renaud[†,*]

[†]*Laboratoire de Microsystemes (LMIS4), Institute of Microengineering, École Polytechnique Fédérale de Lausanne (EPFL), CH-1015 Lausanne, Switzerland.* [§] *School of Materials Science and Engineering and G. W. Woodruff School of Mechanical Engineering, Georgia Institute of Technology, Atlanta, GA, USA.* [‖] *Department of Chemistry, University of Oslo, Oslo 1033 Norway.* [⊥] *Department of Chemical Engineering, Amirkabir University of Technology, Tehran, IR.*

1. Experimental Details

Polybenzimidazole (PBI; Celazole, Hoechst Celanese, Bridgewater, NJ) was dissolved in N,N-dimethylacetamide (DMAc, Aldrich) in a high-pressure reactor under a nitrogen atmosphere and heated to 250 °C at 100 psi pressure for 5 h. Afterwards, the solution cooled to room temperature, and was then filtered.

Microfluidic devices were fabricated with poly(dimethylsiloxane) (PDMS) using the standard micromolding process.[15] To make the master molds, silicon wafers were spin-coated with SU-8 50 photocurable epoxy to a thickness of 60 μm. Baking, lithography, and development procedures were performed at the EPFL center for micronanotechnology (CMi) to obtain negative microchannels on the wafers. The wafers were annealed at 150 ºC to eliminate surface cracks in the SU-8. The resulting molds, after thermal annealing, were treated with a self-assembly monolayer of trimethylethoxy silane by placing a few drops of the chemical under the hood along with the wafers and leaving it for 40 min to prevent the sticking of PDMS to the molds. PDMS (Sylgrad 184) monomer and curing agent were mixed in a weight

ratio of 10:1, poured over the mold, degassed in desiccators and cured in an oven at 80 ºC for 1 h. After curing, the PDMS was removed from the mold and in-/outlet holes were punched using a 150 µm diameter puncher. The PDMS component was then bonded to a glass slide using oxygen plasma (100 mW, 1 min). The resulting device had two inlets for water streams and one for PBI solution, and one outlet. The PBI solution, as the core flow, was squeezed between the two phosphoric acid (H_3PO_4, Aldrich)/water streams at the flow focusing (T-) junction. The mixing channel was 150 µm wide, 60µm high and 1 cm long. The interfacial mixing was controlled by changing the flow ratio of H_3PO_4/water:PBI/DMAc streams from 4 $mL.min^{-1}$:0.1 $mL.min^{-1}$ to 4 $mL.min^{-1}$:0.7 $mL.min^{-1}$.

The produced microfibers were directed to a deionized water bath from end of microfluidic device. After preparation of the microfibers, the majority of the solvent was evaporated in a ventilated oven at temperatures ranging from 60 to 120 °C. The microfibers were then washed with hot water in order to remove the excess phosphoric acid. Finally, the microfibers were dried under vacuum at 160 °C before being subjected to further analysis.

Scanning electron microscopy (SEM; FEI XLF30-FEG) was used at 20 kV accelerating voltage to characterize the PBI based microfibers. The fibers were attached to an SEM grid and coated with a vacuum carbon coater. The images were characterized using ImageJ software based on at least 20 different images. The prepared microfibers in all diameters were quite stable. The SEM imaging of microfibers after three weeks storage in water did not show any significant change in their morphologies.

According to our recent study, by having a dilute PBI solution (0.5-2 mg/ml) and changing the flow ratio, we can generate nanoparticles with different sizes and geometries through a controlled nanoprecipitation process.[15] However, by using more concentrated PBI solutions (5 mg/ml) polymeric chains are in a worm-like state, and by changing the flow regime continuous microfibers are formed.

Differential scanning calorimetry (DSC; Perkin-Elmer) experiments were done on the dried microfibers to measure the glass transition temperature (T_g). In this case, the samples were heated from room temperature to 500°C at a rate of 10 °C.min^{-1}. Reported data are the average of three measurements.

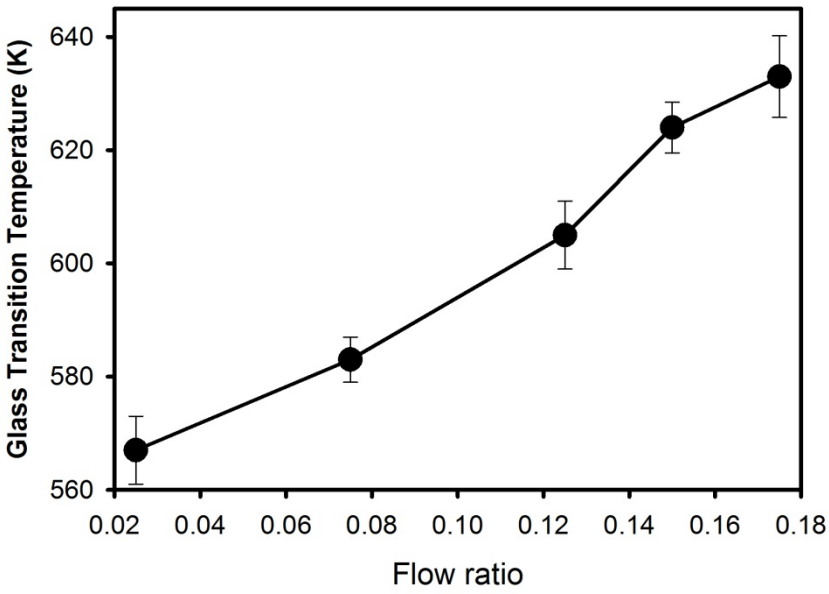

Figure S1. *Glass transition temperature (T_g) of on-chip synthesized phosphoric acid-doped microfibers as a function of flow ratio. The T_g value of phosphoric acid-doped film (40µm thickness) is about 623±8 K.*

The doping level of the microfibers was obtained by means of thermal gravimetric analysis (TGA). TGA analysis was performed on a Mettler Toledo TGA/SDTA 851e. The samples were heated up from 25 to 700 °C at 5 °C/min in an air atmosphere.

Anhydrous proton conductivity of the vacuum dried samples was measured at room temperature. The wet microfiber was placed on four gold electrodes with 2 mm spacing. The gold electrodes were then wire bonded and connected to an electrochemical impedance spectrometer (EIS) for conductivity measurements. Solartron Interface 1260 gain phase analyzer was used over the frequency range of 1-10^6 Hz. The obtained data are reported as the average of at least three samples (Figure 2). The standard deviation (S.D.) was found to be less than 10% for all measurements.

2. Simulation Details

Molecular structures and amorphous cell construction

In the present work, the phosphoric acid (PA) doped PBI microfibers were further studied via all-atom molecular dynamic (MD) simulations to explore their experimentally observed behavior due to PA molecule doping. To this end, four different PA doping levels, λ = 5, 7, 9 and 16, were chosen. Doping level (λ) was defined as the mole ratio of PA molecules to the mole of benzimidazole groups in the PBI structure. Chemical structures of PA molecules and repeat unit of PBI are displayed in scheme S1. PBI chains with degree of polymerization of 50 were considered for simulation. MD simulations were performed on three dimensional (3D) cubic amorphous cells used to represent the behavior of PBI microfibers doped with varied number of PA molecules. These 3D cells consist of PBI polymeric chains and PA molecules, and their compositions are presented in Table 1. To construct the cells, the chemical structure of PA and PBI molecules was first created using Materials Studio software package [29] and then minimized by means of Smart method, available in the Materials Studio software. Subsequently, by using the number of PBI and PA molecules provided in Table 1, initial amorphous 3D cells for the maximum doping level of λ = 16 was built at a very low initial density of 0.005 g/cm^3 using the Amorphous-Cell Builder module. Initial cells for the lower doping levels were created by successive removing the number of PA molecules from the constructed initial cell corresponding to the maximum doping level.

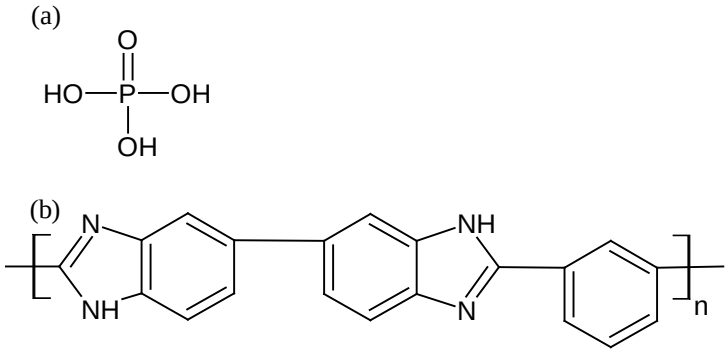

Scheme S1. *Chemical structures of (a) phosphoric acid and (b) PBI monomers used for MD simulations.*

Force field selection and MD simulation

DREIDING force field[30] was employed to describe PBI interactions, which is a general force field dependent on the hybridization rules. This force field has been successfully utilized in the previously reported MD simulations of various hydrated polymeric fuel cell membranes like Nafion, SPEEK and SPPO.[31-34] Partial atomic charges for PBI molecules were determined using the charge equilibration method (QEq) developed by Rappe and Goddard.[35] For PA molecules, interaction parameters were adopted from work by Yan et al..[36] Functional form of the force field has been described in details previously.[34]

MD simulations were performed in two equilibration and production stages. For the equilibration process, the shrinking box procedure was first utilized, which has been discussed elsewhere.[33-34] Equilibration simulation was then continued for 10 ns in NPT ensemble at 1 atm and 433 K to ensure full relaxation of 3D cells and attain the true density of PA-doped PBI systems. The final structure achieved at the end of equilibration was used as the input for the production phase of the MD simulations carried out in NVT ensemble for 2 ns at 433 K. 433 K is the maximum temperature at which doped PBI microfibers were characterized in our experiments, and thus all simulation data presented here are for this temperature. Molecular trajectories from production simulations were used every 1000 time steps for subsequent

structural and dynamical property analysis of PA-doped PBI microfibers. All these MD simulations were performed via LAMMPS (large-scale atomic/molecular massively parallel simulator) open-source classical MD simulation code with the periodic boundary conditions applied in all directions of 3D cells.[37] Non-bonded interactions were truncated at 12 Å cutoff distance and long-range electrostatic interactions were considered using Particle-Particle Particle-Mesh (PPPM) algorithm.[38] Velocity Verlet integrator was used to solve Newton's equation of motion with a time step of 1 fs.[39] Nose-Hoover thermostat and barostat was used to control temperature and pressure with constants of 0.1 and 1 ps, respectively.[40-42]

Table S1. *Composition of the PA-doped PBI microfibers used for MD simulations and calculated average density and cell size for doping levels λ = 5, 7, 9 and 16.*

	Doping level			
	5	7	9	16
No. of PBI chains	2	2	2	2
No. of PA molecules	1000	1400	1800	3200
Total No. of atoms	11604	14804	18004	29204
Density (g/cm^3)	1.5835	1.6057	1.6235	1.6556
Cell size (Å)	51.3128	55.8039	59.6242	70.1673

Amorphous cell equilibrium

Before analyzing the MD simulation results, equilibrium of the amorphous simulation cells was verified through various thermodynamic properties, including density and potential energy. The calculated average density (and cell size) of PA-doped PBI microfibers for all doping levels of PA molecules is summarized in Table 1. It is seen that with an increase in doping level, density is increased due to the higher density of PA molecules as compared to the PBI chains. There has been no experimental density reported in the literature for PBI and PA molecules at 433 K to validate the equilibrated densities obtained from MD simulations.

However, considering the weight percent of PA in the PA-doped PBI systems (i.e., 76, 81.6, 85 and 91% for λ = 5, 7, 9 and 16, respectively), and experimental densities of pure PA (1.89 g/cm^3) and pure untreated PBI fiber (1.2 g/cm^3) at 300 K,[43-44] calculated densities at 433 K were found to be satisfactory. Additionally, the total potential energy was conserved for all doping levels over 2 ns production simulations (not shown here). Consequently, from the computed densities and conservation of potential energy, it can be deduced that the all amorphous cells have become well equilibrated.

Figure 3a illustrates the final microscopic structures of PA-doped PBI for doping levels with λ = 5, 7, 9 and 16. The average cell size of these structures is listed in Table 1. From these configurations, it is generally observed that as the doping level is increased, PBI polymeric chains become more separated, and PA molecules form larger solvent phases. To provide a more detailed understanding concerning these morphological trends of PA-doped PBI materials, microfibers nanostructure, as a function of the PA content, was examined in terms of the correlation between different atoms in PBI and PA molecules, and hydrogen bonding characteristics.

Structural property analysis

Radial distribution function (RDF, also called pair correlation function) $g_{A-B}(r)$ was employed to evaluate the local structure of the doped microfiber. RDF, which indicates the probability distribution of finding B atoms at a distance r with respect to central A atoms, is defined as the following equation:

$$g_{A-B}(r) = \frac{\left(\frac{n_B}{4\pi r^2 \Delta r}\right)}{\left(\frac{N_B}{V}\right)} \tag{5}$$

where n_B is the number of B atoms found around A atoms inside a spherical shell with thickness of Δr, and N_B and V are, respectively, total number of B atoms inside amorphous cells and equilibrated volume of cells.

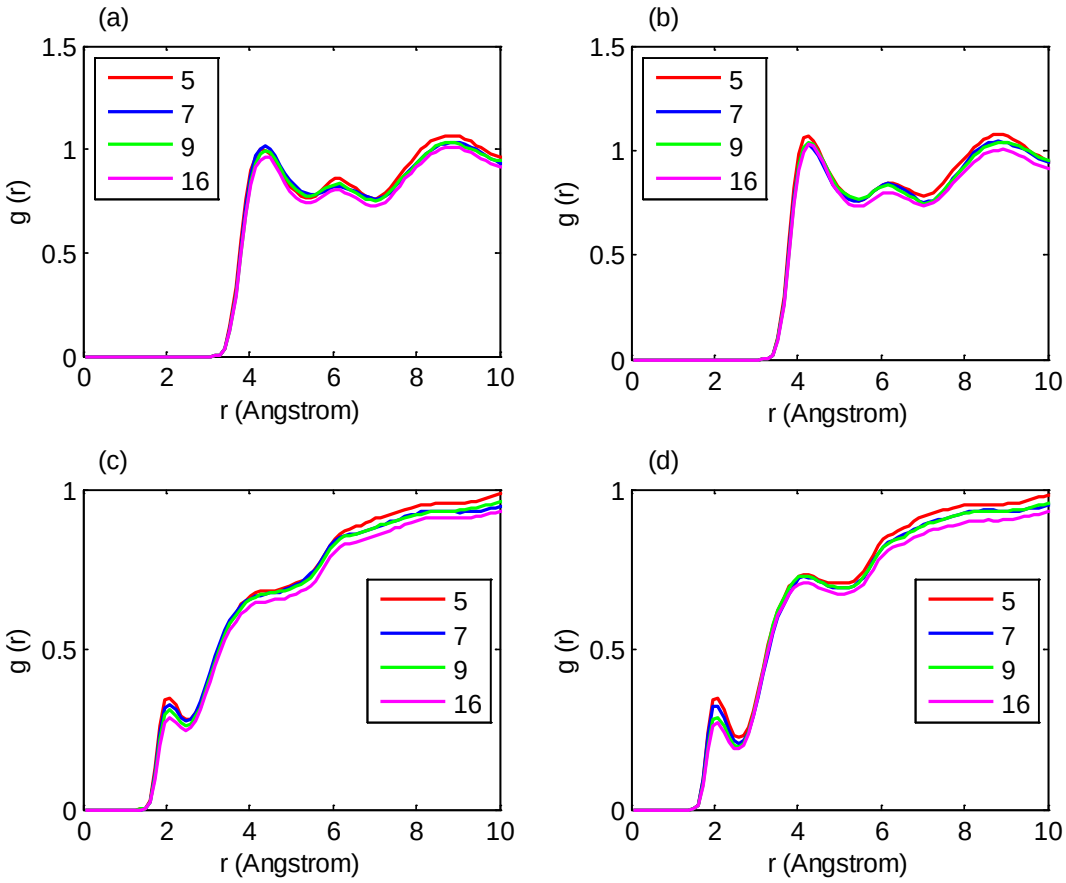

Figure S2. *RDFs of (a) imine nitrogen-phosphorus, (b) amine nitrogen-phosphorus, (c) imine nitrogen-hydrogen (PA), and (d) amine nitrogen-hydrogen (PA) in PA-doped PBI microfibers for doping levels* λ *= 5, 7, 9 and 16.*

Intermolecular interactions between PBI chains and PA solvent molecules were analyzed using RDFs of nitrogen atoms (imine and amine nitrogen, denoted as N2 and N3, respectively) in PBI with regards to phosphorus and hydrogen atoms in PA solvent. Figure

S2a and S2b indicates, respectively, the RDFs of imine nitrogen-phosphorus (N2-P) and amine nitrogen-phosphorus (N3-P) atomic pairs as a function of doping level in PBI microfibers doped with PA. It is observed that the N2-P and N3-P RDFs show the first peak at distances of 4.38 and 4.26 Å, respectively, where peak height in both RDFs does not change much against PA doping level. Peak appearance suggests that PA molecules tend to solvate the PBI chains. This observation is assigned to the hydrogen bonding interactions of imine and amine nitrogen atoms in PBI with PA molecules, which is examined by RDFs of PBI nitrogen atoms with hydrogen atom (denoted as HPA) of PA solvent shown in parts (c) and (d) in Figure S2. It can be seen that both the N2-HAP and N3-HAP intermolecular RDFs exhibit a peak at approximately 2.1 Å, which is in the range of distance required for the hydrogen bond formation. Therefore, the RDFs confirm that PA dopant molecules are able to solvate PBI chains by forming intermolecular hydrogen bonding interactions. Increasing PA doping level leads to a reduction in intensity of observed RDF peaks, which implies that hydrogen bond strength diminishes with increasing doping level.

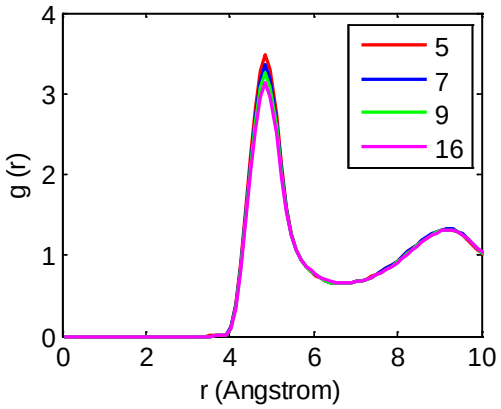

Figure S3*. RDFs between phosphorus atoms of PA molecules in PA-doped PBI microfibers for the doping levels of λ = 5, 7, 9 and 16.*

The visual observation of the existence of a continuous solvent phase within the PA-doped PBI system was examined using calculation of RDFs for phosphorus atoms in PA, as illustrated in Figure S3. For all doping values chosen here for the MD simulation, the P-P

RDFs demonstrate a significant peak at 4.86 Å with a minimum at approximately 6.5 Å. This peak at such RDF is indicative of PA molecules tendency to form the solvent sub-phase. Average coordination number for P-P RDF corresponding to the first solvation shell was estimated to be 9.6, 10.2, 10.6 and 11.3 for λ = 5, 7, 9 and 16 doping levels, respectively. Such findings disclose that with an enhancement in solvent doping level, larger solvent phases are appeared within the microstructure in agreement with visual findings attained from Figure 3a. Solvent phase formation is more likely thanks to hydrogen bonding network among PA solvents. This was probed by HPA atom RDFs with non-protonated (O2) and protonated (O3) oxygen atoms in PA molecules presented in Figure S4. The presence of a peak at 1.62 Å in O2-HAP RDFs, and at 1.74 Å in the case of O3-HAP RDFs, indicates a hydrogen bond in PA solvent molecules. Additionally, higher peak intensity and smaller peak position in O2-HAP RDFs relative to O3-HAP suggests that compared to the protonated oxygen atoms, non-protonated oxygen atoms form stronger hydrogen bonds with the hydrogen atoms in PA molecules.

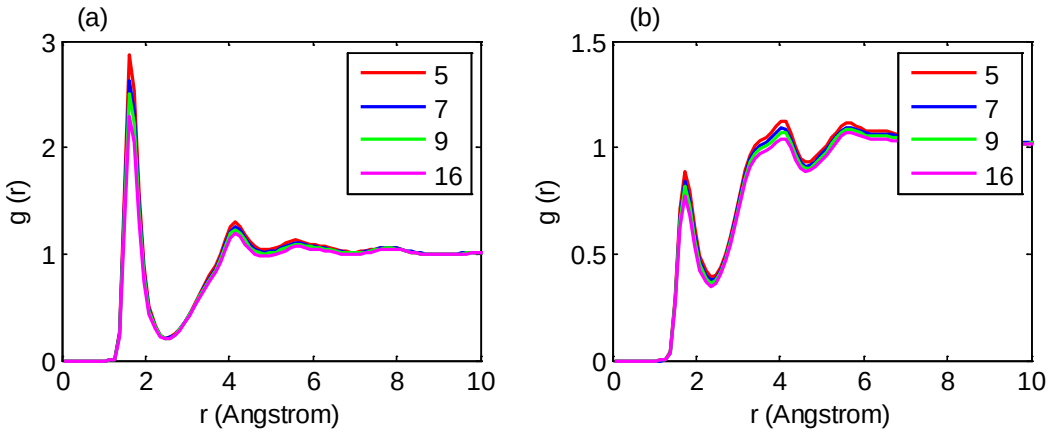

Figure S4. *RDFs of (a) non-protonated oxygen-hydrogen and (b) protonated oxygen-hydrogen of PA molecules in PA-doped PBI microfibers for the doping levels λ = 5, 7, 9 and 16.*

From the above discussions, it can be inferred that hydrogen bonding interactions play a crucial role in PA-doped PBI matrices. Therefore, hydrogen bonding interactions between various pairs of atoms in PA-doped PBI microfibers were evaluated quantitatively by estimating the number of different hydrogen bonds as a function of the PA doping level. In computing the number of hydrogen bonds, a geometric criterion was used. Any two hydrogen bond donor (D) and hydrogen bond acceptor (A) atoms were assumed as hydrogen-bonded with a hydrogen (H) atom if the following conditions are satisfied: (i) the length D…A<3.5 Å, and (ii) the angle D-H…A>120°. The average number of hydrogen bonds calculated according to this geometric condition was collected in Table 2. To better analyze the hydrogen bonding characteristics, the predicted number of hydrogen bonds was normalized with the number of PA molecules corresponding to each doping value (listed in Table 1). As the solvent doping is increased, the average number of hydrogen bonds between PBI molecules (N2-HN interaction), and also between PBI and PA molecules (N2-HPA, O3-HN and O2-HN interactions) is seen to decrease, while that between PA solvents (O3-HPA and O2-HPA interactions) is increased. This behavior suggests that there is a competitive hydrogen bonding interactions in the doped microfibers. The decreasing trend of hydrogen bond number in PBI molecules further reveals the more separation of PBI chains under the condition of increased solvent doping.

Table S2*- Number of hydrogen bonds normalized with the number of PA molecules in PA-doped PBI microfibers for the doping levels of λ = 5, 7, 9 and 16.*

Atomic pair	Doping level (λ)			
	5	7	9	16
N2–HN	0.0051	0.0014	0.0011	0.0005
N2–HPA	0.0677	0.0525	0.0391	0.0220
O3-HN	0.0900	0.0630	0.0514	0.0301
O2-HN	0.0200	0.0156	0.0115	0.0070
O3-HPA	1.9890	2.0576	2.1011	2.1597
O2-HPA	1.1620	1.1824	1.1866	1.2059

Further evidence for existence of PA solvent sub-phases within the PBI microfibers was provided by quantitaive analysis of PA cluster size distribution. For cluster formation, two PA molecules were assumed to be in the same cluster if the distance between their non-protonated oxygen atoms was less than 4.5 Å. This cut-off distance corresponds to the position of the first minimum (the first solvation shell) in O2-O2 RDFs in PA molecules (not shown here). The resulting solvent clusters are very small or large, and thus categorized as small or large cluster in order to better characterize clustering tendency of the PA molecules. Figure S5a and S5b respectively present the small and large cluster size distribution in the term of number of molecules (computed from the average occurrence number of a certain cluster multiplied by its size) vs cluster size, which are average values over 2 ns MD simulations. It is observed that small clusters show similar features at different doping levels, and in the case of large clusters, clusters containing almost all PA solvent molecules were found to appear within the doped matrices. From the sharp distribution of clusters and the trend of increasing cluster size with doping level seen in Figure S5b, it could be deduced that PA clusters in PBI materials containing higher doping levels are better connected compared to those in PBI microfibers with the lower doping levels, in agreement with snapshots provided in Figure 3a. Similar distributions were also found using positions of first minimum in P-P and O3-O3 RDFs as the

cut-off distance criteria. All these structural attributes, which result from hydrogen-bonded PA networks described above lead to the development of continoues solvent subphase, and thereby promote the proton transport characteristics of PA-doped PBI matrix. Similar PA clustering behaviorhave been previoulsly reported by Yan et al. [36] in MD simulation study of Nafion membrane solvated with PA molecules.

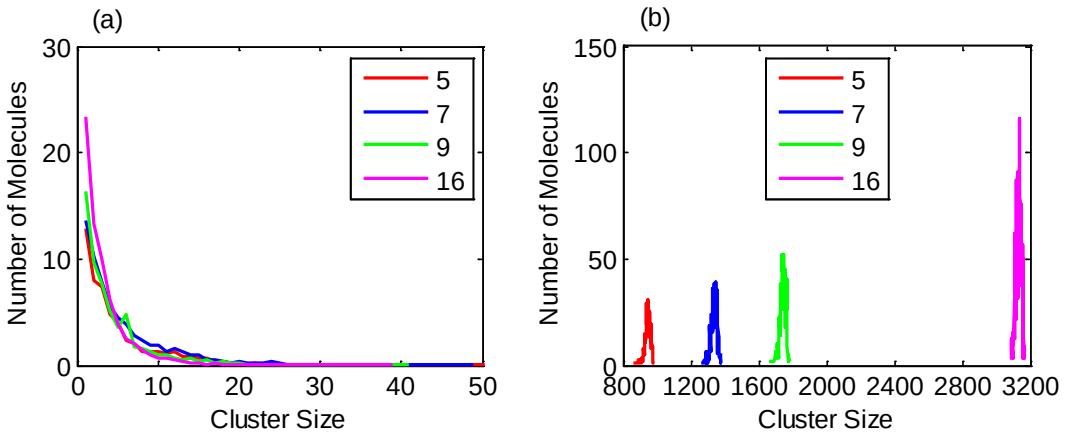

Figure S5*. The average cluster size distribution of PA solvent molecules in PA-doped PBI matrices for the doping levels of λ = 5, 7, 9 and 16 for (a) small and (b) large clusters.*

Dynamical property analysis

Dynamic characteristics of PA-doped microfibers were characterized by calculating the diffusion coefficient for PA molecules within the PBI matrix doped with different amounts of PA solvent. Diffusivity for PA molecules was computed from the slope of their mean squred displacement (MSD) curves (or Einstein relation), mathematically written as follows:

$$D = \frac{1}{6}\lim_{t\to\infty}\frac{dMSD(t)}{dt} = \frac{1}{6N}\lim_{t\to\infty}\frac{d}{dt}\sum_{j=1}^{N}\left[(r_j(t) - r_j(0))^2\right] \quad (2)$$

where $r_j(t)$ and $r_j(0)$ are, respectively, the positions of particle j at time t and at the beginning of the production stage of MD simulations, and N is the total number of particles. Figure 3b demonstrates the MSD of PA molecules for doping levels of λ = 5, 7, 9 and 16 at 433 K. It is seen that MSD for PA molecules inside the PA-doped PBI microfibers is

enhanced as the amount of solvent doping is increased, which shows increased PA mobility within the PBI matrices doped with the higher amounts of PA.

The diffusion coefficients for PA molecules obtained at 433 K based on equation 2 are listed in Table 4 for all the doping levels studied here. Furthermore, it is found that with changing level of PA doping from $\lambda = 5$ to $\lambda = 16$, the MD calculated PA diffusivities through the doped PBI microfibers increased. This trend for simulated diffusion coefficient of PA molecules is consistent with the observations achieved in our experimental results (Figure 3d), and strongly supports the behavior of higher proton conductivity measured under higher PA doping levels.

Table S4*. Simulated diffusion coefficient of PA molecules in the PA-doped PBI microfibers for the doping levels of $\lambda = 5, 7, 9$ and 16.*

Doping level (λ)	D ($\times 10^{-4}$ cm^2/s)
5	0.002667
7	0.004833
9	0.006833
16	0.0111667